Metal-Exchange Catalysis in the Growth of Sesquioxides: Towards Heterostructures of Transparent Oxide Semiconductors

Patrick Vogt,* Oliver Brandt, Henning Riechert, Jonas Lähnemann, and Oliver Bierwagen
Paul-Drude-Institut für Festkörperelektronik, Leibniz-Institut im Forschungsverbund Berlin e.V., Hausvogteiplatz 5–7, 10117 Berlin, Germany
(Received 21 July 2017; published 7 November 2017)

We observe that the growth rate of Ga_2O_3 in plasma-assisted molecular beam epitaxy can be drastically enhanced by an additional In supply. This enhancement is shown to result from a catalytic effect, namely, the rapid formation of In_2O_3, immediately followed by a transformation of In_2O_3 to Ga_2O_3 due to an In-Ga interatomic exchange. We derive a simple model that quantitatively describes this process as well as its consequences on the formation rate of Ga_2O_3. Moreover, we demonstrate that the catalytic action of In_2O_3 allows the synthesis of the metastable hexagonal phase of Ga_2O_3. Since the $Ga_2O_3(0001)/In_2O_3(111)$ interface is closely lattice matched, this novel growth mode opens a new path for the fabrication of sesquioxide heterostructures.

DOI: 10.1103/PhysRevLett.119.196001

The possibility of band gap engineering by fabricating group III–V semiconductor alloys and heterostructures has enabled the development of key technologies such as optoelectronics, telecommunication, and solid-state lighting [1,2]. This technological revolution was based on a few basic material properties. First, the members of a given III–V family share the same crystal structure, with only moderately different lattice constants, allowing the synthesis of heterostructures with coherent interfaces [3]. Second, the binary constituents of most III–V families are chemically miscible to a very high degree, facilitating the growth of alloys with continuously tunable electronic properties [4,5]. Third, the solid composition in many alloys is simply given by the flux ratio in the vapor phase used for their synthesis and can thus be easily controlled and reproduced [6].

The sesquioxides In_2O_3, Ga_2O_3, and Al_2O_3 are an emerging class of materials with unique physical properties. For example, the sesquioxides combine high electrical conductivity with wide band gaps, making them suitable for a variety of novel devices such as deep ultraviolet detectors, transparent transistors, and high power electronics [7,8]. To exploit the potential of this material class, it is highly desirable to transfer the concept of band gap engineering from the III–V compounds to these group III oxides for being able to fabricate, e.g., $(Al_xGa_{1-x})_2O_3/Ga_2O_3$ or $(In_xGa_{1-x})_2O_3/Ga_2O_3$ heterostructures for a large composition range x. However, the sesquioxides crystallize in distinct and epitaxially incompatible equilibrium structures: corundum (rhombohedral, $R\bar{3}c$) for α-Al_2O_3, gallia (monoclinic, $C2/m$) for β-Ga_2O_3, and bixbyite (body center cubic, $Ia\bar{3}$) for In_2O_3 [9–11]. Furthermore, the incorporation of the group III element in sesquioxides is much more complex than for III–V semiconductors. Specifically, the growth rate of the binary sesquioxides is limited by volatile suboxide formation [12,13], restricting the growth conditions to low growth temperatures T_G and mainly to the O-rich regime [14], with detrimental consequences for the crystal quality.

In this Letter, we report on a novel mechanism which circumvents suboxide formation and lifts the rigid constraints on the conditions under which the synthesis of Ga_2O_3 films is possible. Using an additional flux of In ϕ_{In} during the plasma-assisted molecular beam epitaxy (PAMBE) of Ga_2O_3, we observe that the growth rate $\Gamma_{Ga_2O_3}$ of Ga_2O_3 is drastically enhanced. It remains high even for T_G, for which Ga_2O_3 does not form at all in the absence of In. We show that this phenomenon is caused by the rapid formation of In_2O_3 followed by an exchange of In in In_2O_3 by Ga adatoms. Indium adatoms released by this reaction can be reoxidized, and In_2O_3 hence acts as a catalyst for the growth of Ga_2O_3. This metal-exchange catalysis allows us to synthesize Ga_2O_3 in its metastable hexagonal modification. The resulting ε-$Ga_2O_3(0001)$ films are of high crystal quality and are shown to be crystallographically compatible with the bixbyite structure of In_2O_3.

All samples were grown on α-$Al_2O_3(0001)$ by means of PAMBE. A 20 nm thick Ga_2O_3 nucleation layer was grown first to exclude effects by nucleation processes. Growth rates and desorption rates were measured *in situ* by laser reflectometry (LR) and line-of-sight quadrupole mass spectrometry (QMS), respectively. The Ga flux ϕ_{Ga} was 6.5 $nm^{-2}\,s^{-1}$, and ϕ_{In} was varied from 0 to 4.0 $nm^{-2}\,s^{-1}$. The activated O fluxes ϕ_O delivered by a radio-frequency plasma cell, $\phi_O = \eta\phi_O^{net}$ (with net O flux ϕ_O^{net}), ϕ_{Ga}, and ϕ_{In}, were calibrated following the procedure reported in Refs. [12–15]. The oxidation efficiency η is defined as the fraction of the maximum available O adatoms for metal oxidation at a given ϕ_O^{net}. The relative oxidation efficiency between In and Ga has been determined to be $\eta_{In} \approx 2.8\eta_{Ga}$ [16]. Hence, the ϕ_O available for In and Ga is 19.2 $nm^{-2}\,s^{-1}$ and 6.7 $nm^{-2}\,s^{-1}$ [16], respectively. T_G

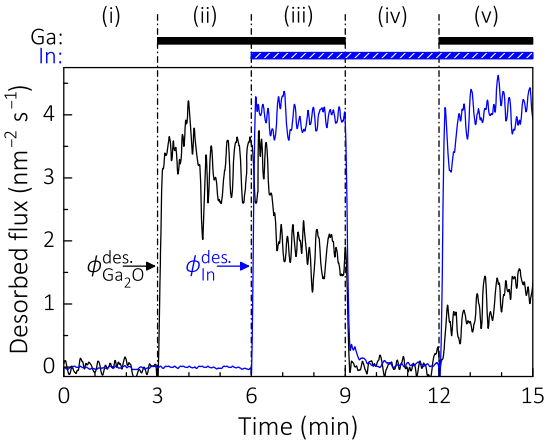

FIG. 1. Desorption of Ga_2O and In from a β-$Ga_2O_3(\bar{2}01)$ surface at $T_G = 700$ °C, $\phi_{Ga} = 6.5$ nm^{-2} s^{-1}, and $\phi_{In} = 4.0$ nm^{-2} s^{-1}. The metals supplied in the time intervals (i)–(v) are indicated by the bars at the top.

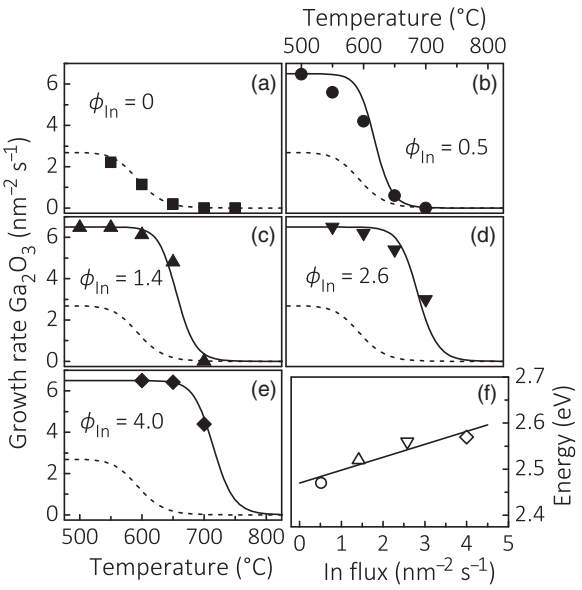

FIG. 2. (a)–(e) T_G dependence of $\Gamma_{Ga_2O_3}$. ϕ_{In}, supplied for each set of experiments, is indicated in the figures in units of nm^{-2}s^{-1}. The symbols represent experimental data and the solid lines are fits to Eq. (6). The dashed line is a guide for the eye. (f) Activation energy of In desorption as a function of ϕ_{In}. The symbols represent experimental data and the solid line is a fit of the data to Eq. (8).

was calibrated using QMS by detecting the total desorption of a known metal flux following the procedure described in Ref. [17]. The composition and the crystallinity of the films were measured *ex situ* by energy dispersive x-ray spectroscopy (EDX) in a scanning electron microscope with an uncertainty of 1%, as well as longitudinal (ω-2θ) and transverse (ω) x-ray diffraction (XRD) scans, respectively.

Figure 1 shows the flux of Ga_2O ($\phi^{des}_{Ga_2O}$) and In (ϕ^{des}_{In}) desorbing from β-Ga_2O_3 template as measured by QMS at $T_G = 700$ °C. During the initial time interval (i), the surface was exposed only to ϕ_O, and no desorption of metal species takes place. In time interval (ii), ϕ_{Ga} was also supplied to the surface. At this T_G, no Ga_2O_3 growth takes place, as evidenced by LR [16]. Instead, Ga reacts with O, forming the volatile suboxide Ga_2O [12,14]. The desorption flux of Ga_2O indeed accounts for the total ϕ_{Ga} supplied. In time interval (iii), ϕ_{In} is supplied in addition to ϕ_{Ga} and ϕ_O. After a short delay, the Ga_2O desorption flux decreases by 40%, and LR evidences the growth of Ga_2O_3 [16]. At this T_G, all In supplied to the surface desorbs in agreement with the absence of In in the Ga_2O_3 film, as measured by *ex situ* EDX. When the Ga shutter is closed in time interval (iv), In desorption ceases as In_2O_3 nucleates immediately, and, in combination with LR, complete In incorporation is observed and the growth rate of In_2O_3 corresponds to ϕ_{In}. Once the Ga shutter is opened again in time interval (v), Ga_2O_3 growth sets in again with $\Gamma_{Ga_2O_3} = 4.4$ nm^{-2} s^{-1} on In_2O_3, and In desorbs simultaneously. This sequence of experiments shows most clearly that the additional In has a catalytic effect on the formation of Ga_2O_3: it enables the growth of Ga_2O_3 under conditions where Ga_2O_3 will not form at all in the absence of In. This effect should not be confused with that of a surfactant, which either inhibits [18] or induces [19] a morphological phase transition but does not affect the growth rate of the material.

Figures 2 and 3 summarize the measured $\Gamma_{Ga_2O_3}$ as a function of T_G at different ϕ_{In}'s, and as a function of ϕ_{In} at different T_G's, respectively. Both figures contain the same data, but they are complementary in that they allow us to separately examine the effects of T_G and ϕ_{In} on $\Gamma_{Ga_2O_3}$. *Ex situ* EDX measurements confirm that no In was incorporated into the entire parameter space. The data in Fig. 2(a) correspond to the values of $\Gamma_{Ga_2O_3}$ in the absence of In at otherwise identical growth conditions. Here, $\Gamma_{Ga_2O_3}$ decreases with an increasing T_G due to Ga_2O desorption [14]. Evidently, additional ϕ_{In} enhances $\Gamma_{Ga_2O_3}$ significantly—even at the lowest T_G—and enables the growth at a higher T_G. This effect is stronger the higher ϕ_{In} is, as can be seen in Fig. 3: with increasing ϕ_{In}, $\Gamma_{Ga_2O_3}$ monotonically increases until it saturates at ϕ_{Ga}, corresponding to complete Ga incorporation. Note that $\Gamma_{Ga_2O_3}$ can exceed ϕ_{In}, demonstrating that a fraction of In atoms released by the In-Ga exchange process is reoxidized.

Based on the understanding of the factors governing the growth of Ga_2O_3 acquired in our previous work, we explain this observation as a two-step reaction. Because of the higher η of In compared to Ga [16], the formation of In_2O_3 is kinetically favored; i.e., In adatoms are faster to react with the impinging ϕ_O than Ga adatoms are. Hence, In_2O_3 is formed predominantly in this first step of the reaction. However, In_2O_3 is unstable in the presence of Ga, as it is energetically favorable to replace In by Ga in the In–O bonds [15]. An analogous instability of In_2O_3 in the presence of Fe was recently reported and was shown to

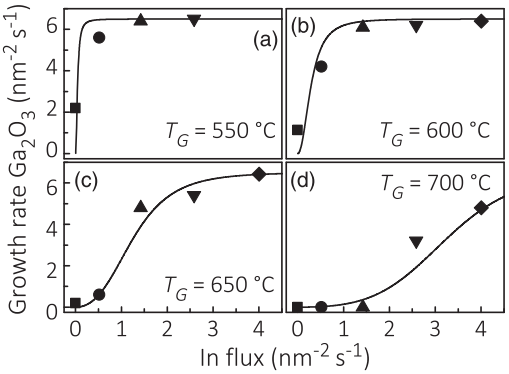

FIG. 3. Dependence of $\Gamma_{Ga_2O_3}$ on ϕ_{In} for different T_G's, as indicated in the figures. The symbols represent experimental data and the solid lines are model predictions by Eqs. (6)–(8).

result in In adatoms on the oxide surface after deposition of Fe and the subsequent In-Fe exchange [20]. Similarly, Ga exchanges In in our case, using the O reacted with In_2O_3 as a reservoir, while transferring the exchanged In to the oxide surface. In this way, the formation of the volatile suboxide Ga_2O is bypassed, allowing Ga_2O_3 to be grown at an elevated T_G and at nominally Ga-rich conditions. Depending on the surface lifetime of In adatoms, they can be reoxidized to In_2O_3, and subsequently exchanged by other Ga adatoms. This reoxidation step principally enables $\Gamma_{Ga_2O_3}$ to exceed ϕ_{In}, as was indeed experimentally observed. The consecutive catalytic reaction including the initial formation of In_2O_3 and the subsequent In-Ga exchange, constituting the metal-exchange oxide growth, thus reads

$$2\mathrm{In}(a) + 3\mathrm{O}(a) \rightarrow \mathrm{In_2O_3}(s), \tag{1}$$

$$2\mathrm{Ga}(a) + \mathrm{In_2O_3}(s) \rightarrow \mathrm{Ga_2O_3}(s) + 2\mathrm{In}(a). \tag{2}$$

The adsorbate and solid phases are denoted as a and s, respectively.

To quantitatively determine the $\Gamma_{Ga_2O_3}$ resulting from reactions (1) and (2), we set up a simple rate-equation model. In principle, we would have to take into account the adatom populations of In, Ga, and O, together with the densities for In_2O_3 and Ga_2O_3. The resulting system of coupled equations would be highly complex and accessible only to a numerical approach. We can reduce the complexity considerably by taking into account the most likely reaction mechanisms governing the formation of In_2O_3 and Ga_2O_3. For the former, the highly reactive—and equally volatile—O radicals created by the plasma source are not expected to form a stable adlayer, but In adatoms are, rather, reacting directly with an impinging ϕ_O (Eley-Rideal reaction mechanism [21]). For the latter, we note that, in the absence of In, we do not observe any desorption of elemental Ga from the surface even at the highest T_G involved, suggesting that suboxide formation inhibits the accumulation of a significant steady-state concentration of Ga adatoms. In the presence of In, the efficient oxidation of In outperforms suboxide formation, and the Ga adatom population should be decreased even further. We thus write

$$\frac{dn_{In}}{dt} = 0 = \phi_{In} - \sigma^2\phi_O n_{In}^2(1-\theta) + \alpha\phi_{Ga}\theta - \gamma n_{In}, \tag{3}$$

$$\frac{d\theta}{dt} = 0 = \sigma^2\phi_O n_{In}^2(1-\theta) - \alpha\phi_{Ga}\theta, \tag{4}$$

with the In adatom density n_{In} and the surface coverage θ of In_2O_3. The second and third terms of Eq. (3) are the formation rates of In_2O_3 and Ga_2O_3, respectively. Note that reoxidation of In released by the In-Ga exchange is automatically taken into account by the presence of the third term in Eq. (3). The factor $(1-\theta)$ assures that In_2O_3 constitutes a surface and not a bulk phase [22]. Finally, the last term of Eq. (3) accounts for In desorption with the desorption rate constant γ. The quantity σ has the dimension nm^2, representing the cross section of the reaction between colliding In and O atoms. The prefactor α is dimensionless and ranges principally between 0 and 1. In the present case, no In is incorporated, reactions (1) and (2) are in balance, and $\alpha = 1$. Thus, $\Gamma_{Ga_2O_3}$ is given by

$$\Gamma_{Ga_2O_3} = \phi_{Ga}\theta. \tag{5}$$

Solving Eqs. (3) and (4) with respect to n_{In} and θ yields $\phi_{In} = \gamma n_{In}$, as was experimentally observed for the data plotted in Figs. 1, 2, and 3; i.e., there is no measured In incorporation or accumulation. Inserting the solution for θ into Eq. (5) yields the following expression for $\Gamma_{Ga_2O_3}$ in the presence of ϕ_{In}:

$$\Gamma_{Ga_2O_3} = \frac{\phi_{Ga}\phi_O{\phi_{In}}^2}{J^2\phi_{Ga} + {\phi_{In}}^2\phi_O}. \tag{6}$$

The only free parameter $J = \gamma/\sigma$ has the dimension of a reaction rate. We assume that its dependence on T_G can be written

$$J = \frac{\gamma}{\sigma} = J_0 \exp\left(-\frac{\Delta}{k_B T_G}\right), \tag{7}$$

with the activation energy Δ and the Boltzmann constant k_B. Based on the collision theory of adsorbed gases with the covalent radii of In and O atoms taken as hard spheres, the preexponential factor J_0 is estimated to be on the order of 1×10^{14} nm^{-2} s^{-1}. Note that the value of Δ deduced below does not depend sensitively on the magnitude of J_0. Allowing the value of Δ to be freely adjustable, we perform least-square fits of the data by Eq. (6) depicted by the solid lines in Figs. 2(b)–2(e). The values of Δ obtained by these fits are plotted in Fig. 2(f). A linear fit with

$$\Delta(\phi_{In}) = \Delta_0 + \Sigma_\Delta\phi_{In} \tag{8}$$

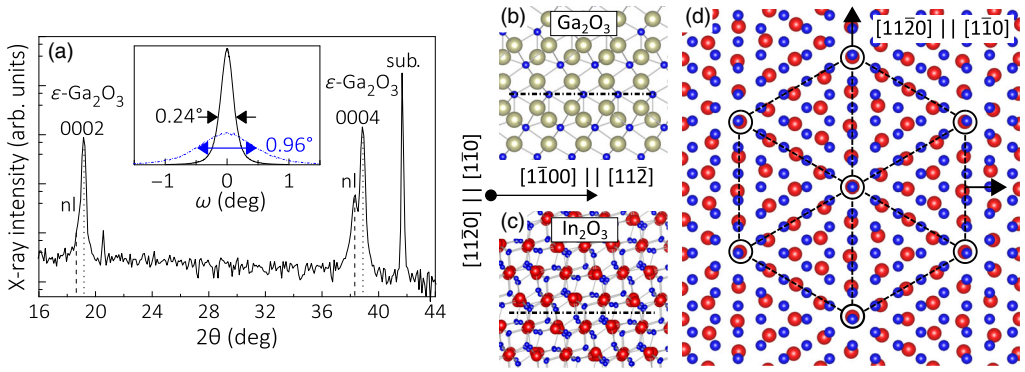

FIG. 4. (a) Longitudinal XRD scan recorded from an In_2O_3-catalyzed Ga_2O_3 film grown on a β-$Ga_2O_3(\bar{2}01)$/α-$Al_2O_3(0001)$ template at $T_G = 700$ °C, $\phi_{Ga} = 6.5$ nm^{-2} s^{-1}, and $\phi_{In} = 5.4$ nm^{-2} s^{-1}. Reflections labeled "sub." and "nl" stem from the substrate [α-$Al_2O_3(0006)$] and the nucleation layer [β-$Ga_2O_3(\bar{2}01)$ and $(\bar{4}02)$], respectively. The reflections from the Ga_2O_3 film are identified to originate from the metastable ε phase, as indicated in the figure. (Inset) Transverse scans across the ε-$Ga_2O_3(0004)$ (solid black line) and ε-$Ga_2O_3(10\bar{1}4)$ (dashed-dotted blue line) reflections. The full width at half maxima of the reflections are indicated in the figure. (b), (c) Side view of the ε-$Ga_2O_3(0001)$ and $In_2O_3(111)$ planes, respectively. The dashed-dotted lines indicate the bulk-terminated surfaces. The Ga, In, and O atoms are depicted in gold, red, and blue, respectively. (d) Top view of ε-$Ga_2O_3(0001)$ and $In_2O_3(111)$. The dashed lines illustrate a 5:4 coincidence lattice of O-terminated ε-$Ga_2O_3(0001)$ relative to In-terminated $In_2O_3(111)$.

yields $\Delta_0 = \Delta(\phi_{In} = 0) = (2.47 \pm 0.02)$ eV and $\Sigma_\Delta = (28 \pm 7)$ meV nm^2 s. The same values were taken for the model predictions of the data in Fig. 3.

Within experimental uncertainty, Δ_0 corresponds to the vaporization enthalpy of elemental In, which is known to be (2.40 ± 0.12) eV [23]. This result suggests that the desorption process is only weakly affected by the fact that desorption takes place from a Ga_2O_3 surface. Still, the presence of other species on the surface, such as O and Ga, will influence the desorption kinetics of In depending on the surface coverage [24,25]. In the regime we are concerned with, $n_{In} \propto \phi_{In}$, and the average adsorbate-adsorbate binding lengths will thus decrease with an increasing ϕ_{In}, affecting their binding energy such that Δ increases with an increasing ϕ_{In}. Analogous behavior has also been observed for the desorption kinetics of Ga on GaN [26].

As a unique benefit of the metal-exchange catalysis, we are able to explore PAMBE growth regimes for the synthesis of Ga_2O_3 films which were previously inaccessible. Figure 4(a) shows an ω-2θ XRD scan of a Ga_2O_3 film. The reflections of the film do not coincide with those of the nucleation layer, but they are clearly shifted to larger angles. The angular position of these reflections perfectly agrees with those of the 0002 and 0004 reflections of the metastable ε-Ga_2O_3 phase, which crystallizes in a hexagonal structure ($P6_3mc$ [27]). This assignment is confirmed by azimuthal XRD scans of the asymmetric $10\bar{1}4$ reflection, and electron backscatter diffraction reveals that the film is single phase ε-Ga_2O_3 [16], even on a nanometer scale. The inset of Fig. 4(a) shows transverse scans across the symmetric 0004 and asymmetric $10\bar{1}4$ reflections of ε-Ga_2O_3. The width of the profiles is a measure for the out-of-plane and in-plane orientation distribution. Clearly, the profiles reveal a well-oriented epitaxial film, which is particularly remarkable since films in the ε phase could not yet be obtained by PAMBE.

ε-Ga_2O_3 films, such as the one synthesized by the In_2O_3-catalyzed high-T_G growth in this Letter, are of considerable interest for the realization of ε-$Ga_2O_3(0001)$/$In_2O_3(111)$ heterostructures since the symmetry of these planes matches. Figures 4(b) and 4(c) show side views of the (0001) and (111) surfaces of ε-Ga_2O_3 and In_2O_3, respectively. The former exhibits a stacking alternating between stoichiometric bi- and trilayers along the $\langle 0001 \rangle$ direction, while the latter consists of a sequence of stoichiometric trilayers stacked along the $\langle 111 \rangle$ direction. A virtual cleavage of the two structures along the dashed lines in Figs. 4(b) and 4(c) and superimposing the resulting bulk-terminated surfaces results in the interfacial arrangement shown in Fig. 4(d). Evidently, the ε-$Ga_2O_3(0001)$ surface is well matched—in symmetry, atomic spacing, and surface chemistry—to bixbyite $In_2O_3(111)$. As indicated by the dashed lines in Fig. 4(d), the two lattices are in almost perfect registry when forming a 5:4 coincidence lattice with a residual mismatch of 1.3%.

This situation is similar to the one encountered in the growth of InN(0001) films on $In_2O_3(111)$ [28], where a 4:1 coincidence lattice with a residual mismatch of 1% was found to enable the synthesis of InN(0001) films with atomically abrupt InN/In_2O_3 interfaces, high structural perfection, and intense room temperature luminescence. We envision that the crystallographic match between ε-$Ga_2O_3(0001)$ and $In_2O_3(111)$ will allow the fabrication of sesquioxide heterostructures with coherent interfaces. In addition, the structural similarity between the hexagonal modification of Ga_2O_3 and the bixbyite structure of In_2O_3 may facilitate the synthesis of homogeneous $(In_xGa_{1-x})_2O_3$ alloys with a significant In

content, where In incorporation is promoted by a sufficiently high ϕ_O [15].

We point out that the metal-exchange catalysis discovered in this work should apply to all materials whose binary constituents exhibit analogous kinetic and thermodynamic properties to those discussed above for In_2O_3 and Ga_2O_3. For example, we recently showed that the oxidation efficiency of Sn (η_{Sn}) is even larger than that of In, which, in turn, is larger than that of Ga, i.e., $\eta_{Sn} > \eta_{In} > \eta_{Ga}$ [12]. Thus, we expect catalytic effects for a wide range of ternary oxide alloys, but also for various other multicomponent oxides fabricated by MBE [29].

Finally, the discovered metal-exchange mechanism opens a new path for the epitaxial synthesis of transparent semiconducting oxides. If successful, the developments presented will open a new path for the band gap engineering and heterostructural growth of these materials.

We thank Hans-Peter Schönherr for his technical MBE support, Uwe Jahn for his EDX assistance, and Vladimir Kaganer for his critical reading of the manuscript. This work was performed in the framework of GraFOx, a Leibniz-Science Campus partially funded by the Leibniz Association.

*vogt@pdi-berlin.de

[1] H. Kroemer, Rev. Mod. Phys. **73**, 783 (2001).
[2] S. Nakamura, Rev. Mod. Phys. **87**, 1139 (2015).
[3] S. Adachi, J. Appl. Phys. **58**, R1 (1985).
[4] K. Ploog, Annu. Rev. Mater. Sci. **12**, 123 (1982).
[5] M. J. Manfra, Annu. Rev. Mater. Sci. **5**, 347 (2014).
[6] K. Ploog, Annu. Rev. Mater. Sci. **11**, 171 (1981).
[7] M. Higashiwaki, K. Sasaki, H. Murakami, Y. Kumagai, A. Koukitu, A. Kuramata, T. Masui, and S. Yamakoshi, Semicond. Sci. Technol. **31**, 034001 (2016).
[8] O. Bierwagen, Semicond. Sci. Technol. **30**, 024001 (2015).
[9] M. Marezio, Acta Crystallogr. **20**, 723 (1966).
[10] L. M. Foster, G. V. Chandrashekhar, J. E. Scardefield, and R. B. Bradford, J. Am. Ceram. Soc. **63**, 509 (1980).
[11] F. P. Sabino, L. N. de Oliveira, and J. L. F. Da Silva, Phys. Rev. B **90**, 155206 (2014).
[12] P. Vogt and O. Bierwagen, Appl. Phys. Lett. **106**, 081910 (2015).
[13] P. Vogt and O. Bierwagen, Appl. Phys. Lett. **109**, 062103 (2016).
[14] P. Vogt and O. Bierwagen, Appl. Phys. Lett. **108**, 072101 (2016).
[15] P. Vogt and O. Bierwagen, APL Mater. **4**, 086112 (2016).
[16] See Supplemental Material at http://link.aps.org/supplemental/10.1103/PhysRevLett.119.196001 for experiments regarding the oxidation efficiencies, *in situ* laser reflectometry, and electron backscatter diffraction scans.
[17] R. Held, D. E. Crawford, A. M. Johnston, A. M. Dabiran, and P. I. Cohen, Surf. Rev. Lett. **05**, 913 (1998).
[18] M. Copel, M. C. Reuter, E. Kaxiras, and R. M. Tromp, Phys. Rev. Lett. **63**, 632 (1989).
[19] R. B. Lewis, P. Corfdir, H. Li, J. Herranz, C. Pfüller, O. Brandt, and L. Geelhaar, Phys. Rev. Lett. **119**, 086101 (2017).
[20] M. Wagner, P. Lackner, S. Seiler, S. Gerhold, J. Osiecki, K. Schulte, L. A. Boatner, M. Schmid, B. Meyer, and U. Diebold, Phys. Rev. Lett. **117**, 206101 (2016).
[21] D. D. Eley and E. K. Rideal, Nature (London) **146**, 401 (1940).
[22] O. Brandt, H. Yang, and K. H. Ploog, Phys. Rev. B **54**, 4432 (1996).
[23] C. B. Alcock, V. P. Itkin, and M. K. Horrigan, Can. Metall. Q. **23**, 309 (1984).
[24] V. P. Zhdanov, J. Chem. Phys. **114**, 4746 (2001).
[25] C. Stampfl, H. J. Kreuzer, S. H. Payne, H. Pfnür, and M. Scheffler, Phys. Rev. Lett. **83**, 2993 (1999).
[26] L. He, Y. T. Moon, J. Xie, M. Muñoz, D. Johnstone, and H. Morkoç, Appl. Phys. Lett. **88**, 071901 (2006).
[27] F. Mezzadri, G. Calestani, F. Boschi, D. Delmonte, M. Bosi, and R. Fornari, Inorg. Chem. **55**, 12079 (2016).
[28] S. Sadofev, Y. Cho, O. Brandt, M. Ramsteiner, R. Calarco, H. Riechert, S. C. Erwin, Z. Galazka, M. Korytov, M. Albrecht, R. Uecker, and R. Fornari, Appl. Phys. Lett. **101**, 172102 (2012).
[29] D. G. Schlom, APL Mater. **3**, 062403 (2015).